Effects of the Guiding Tank on Flow Characteristics inside the Double-Suction Squirrel-Cage Fan for Range Hood

International Journal of Fluid Machinery and Systems
Vol. 13, No. 1, January-March 2020

DOI: http://dx.doi.org/10.5293/IJFMS.2020.13.1.203
ISSN (Online): 1882-9554

Original Paper

Effects of the Guiding Tank on Flow Characteristics inside the Double-Suction Squirrel-Cage Fan for Range Hood

Yingkun Zhang[1], Kunhang Li[1], Yunlong Li[1] and Jingyin Li[1]

[1]School of Energy and Power Engineering, Xi'an Jiaotong University
28 West Xianning Road, Xi'an, 710049, China, yingkunz@163.com, kunhangli@stu.xjtu.edu.cn, liyunlong2@stu.xjtu.edu.cn, jyli@mail.xjtu.edu.cn

Abstract

The effects of the guiding tank on flow characteristics inside a double-suction squirrel-cage fan for the range hood were numerically investigated in this paper. Flow analysis was conducted by solving the three-dimensional steady Reynolds-averaged Navier-Stokes equations using the realizable k-ε turbulence model. Numerical results were validated with the experimental data for total pressure. Differences in flow characteristics between the fan model and the range hood model at the nearly maximum mass flow rate of 0.3214 kg/s were analyzed in detail. Numerical simulation results show that the incoming flow of the squirrel-cage fan will be distorted due to the guiding tank. The inlet distortion will deteriorate the aerodynamic performance of the squirrel-cage fan and cause obvious differences in the velocity field, the pressure field and the vortex structures inside the fan.

Keywords: Range hood, Guiding tank, Inlet distortion, Flow characteristics

1. Introduction

The range hood, an important household appliance, is facing an increasing demand for the higher aerodynamic performance, such as the higher flow rate, the lower noise and so on. Due to its limited space, only the squirrel-cage fan can meet the strict requirements. The single-suction squirrel-cage fan is firstly applied to the range hood, and its aerodynamic performance has been studied by many researchers. For example, Heo et al. [1] improved the efficiency of a squirrel-cage fan through a radial basis neural network surrogate model with four design variables defining the volute cut-off angle, volute diffuser expansion angle, impeller diameter ratio, and impeller exit angle. Gholamian et al. [2, 3] numerically investigated the effects of collector diameters on flow characteristics of squirrel-cage fans and the results indicated that an appropriate collector outlet diameter led to the suitable axial velocity and improved the flow at the entrance of impeller. Darvish et al. [4] applied the stepped volute tongue to the squirrel-cage fan and reduced the aerodynamic noise of the fan. Besides, experiments are also performed to investigate the flow in squirrel-cage fans. For example, Velarde et al. [5] adopted the hot wire techniques to obtain steady velocity components and velocity unsteadiness levels of a squirrel-cage fan and the data revealed a strong flow asymmetry with considerable changes in both magnitude and direction along circumferential positions. Samian et al. [6] studied the velocity distribution of a single-suction squirrel-cage fan using the laser doppler anemometry and found that the narrower impeller suppressed the secondary flow vortex near the shroud effectively. Kang et al. [7] investigated flow characteristics of a squirrel-cage fan using PIV measurement and total pressure probes and found that the stagnation point at cut-off region of the fan moved to the exit of the volute as the cut-off angle increased. Further, the double-suction squirrel-cage fan, which meets the need of increasing the mass flow rate requirement, is becoming popular in the range hood. Therefore, the flow fields inside the double-suction squirrel-cage fan have also attracted more and more interests of researchers. Ballesterostajadura et al. [8] numerically studied the unsteady flow fields inside a double-suction squirrel-cage fan and found that the velocity of the obstructed inlet impeller is less than that of the free inlet impeller. Zhang et al. [9] improved the total pressure of a double-suction squirrel-cage fan through response surface method by optimizing the impeller inlet angle, impeller outlet angle and impeller diameter ratio.

The above studies mainly focused on the aerodynamic performance of the fan with the uniform incoming flow. However, for the range hood, the incoming flow of the squirrel-cage fan must be deflected seriously due to the existence of the guiding tank. As Iwamoto et al. [10] studied, the deflected inflow will induce the regions with strong unsteadiness shrink in peripheral direction and extend in axial direction. Montazerin [11] also indicated that the incoming flow direction has a significant effect on the aerodynamic performance of the squirrel-cage fan. Besides, the deflected incoming flow of the guiding tank may produce more

Received February 7 2019; revised April 8 2019; accepted for publication October 10 2019:
Review conducted by Tong Seop Kim. (Paper number O19009K) Corresponding author: Jingyin Li, jyli@mail.xjtu.edu.cn

flow losses and obvious inlet distortions to the squirrel-cage fan inside the range hood. Some related studies have revealed that the inlet distortion will deteriorate the fan's aerodynamic performance. For example, Wang et al. [12] investigated the inlet distortion effects on the aerodynamic performance of a centrifugal fan and the results showed that the inlet distortion decreases the centrifugal fan pressure and efficiency by 200 Pa and 6.5% respectively compared with the uniform incoming flow. Zhang et al. [13] also found that the inlet distortion didn't only degrade the aerodynamic performance of the compressor, but also decreased the stability clearly.

In addition, many researchers mainly focus on the fan aerodynamic performance at the design load. However, for the range hood, the larger mass flow rate will produce the greater exhaust smoke volume, which will make the kitchen clean more quickly. Therefore, the aerodynamic performance of the range hood under the large mass flow rate is important. Obviously, flow fields inside the fan at off-design load are different from that for the design load. For example, Cheah et al. [14] found that the uniform flow developed at the design flow rate and the pre-rotation flow developed upstream at higher flow rates. As reported by Pedersen et al. [15], the smooth flow in the impeller at the design load changed into a stalled flow at the off-design point load.

In this paper, effects of the guiding tank on flow characteristics inside a double-suction squirrel-cage fan for the range hood are numerically investigated. Two models are introduced in sect. 2. One is the fan model, including the inlet tubes, the squirrel-cage fan and the ventilation duct; another one is the range hood model, including the guiding tank, the squirrel-cage fan and the ventilation duct. Numerical methods of the two models and the experimental apparatus of the range hood model are introduced in sect. 3. In sect. 4.1, the numerical results are validated with the experimental data and the aerodynamic performances of the two models under various mass flow rates are also compared. In sect. 4.2, the flow characteristics under a large mass flow rate of 0.3214 kg/s are carefully investigated. Differences in the velocity field, the pressure field and the vortex structures between the fan model and the range hood model are presented in detail. This paper ends with conclusions in sect. 5. The results show that the guiding tank will cause obvious inlet distortions, which would influence the flow characteristics and the aerodynamic performance of the squirrel-cage fan inside the range hood model significantly.

2. Models

The range hood model, as shown in Figs. 1 and 2, is composed of a guiding tank, a squirrel-cage fan and a ventilation duct. The guiding tank, working as the inlet box, will guide the flow into the fan. Due to the guiding tank, the incoming flow of the fan would be distorted and thus it would lead to additional flow losses and deteriorate internal flow inside the fan.

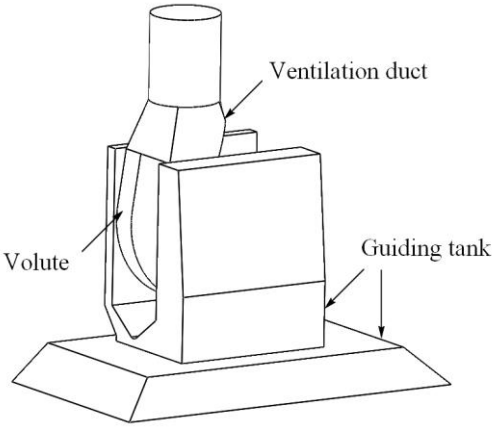

Fig. 1 General view of the range hood model

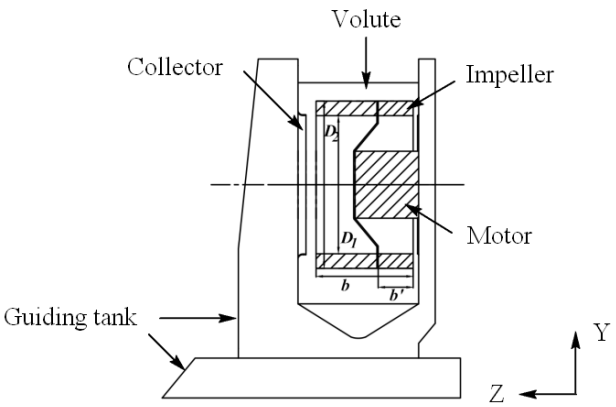

Fig. 2 Side view of the range hood model

The fan model, as shown in Fig. 3, is composed of the same squirrel-cage fan and ventilation duct as the range hood model. Besides, the two straight extended inlet tubes are added, which will provide more uniform incoming flow for the squirrel-cage fan compared to the guiding tank mentioned above.

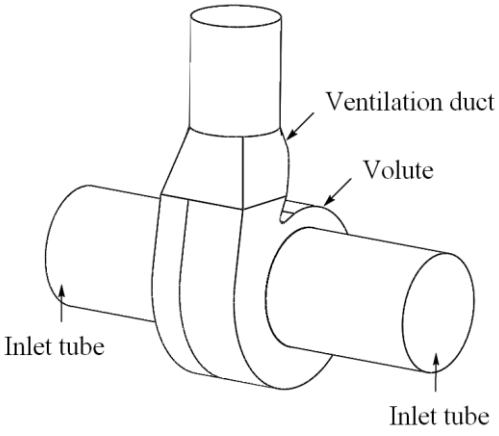

Fig. 3 General view of the fan model

The squirrel-cage fan under investigation is a double-suction squirrel-cage fan. It has 60 forward-curved blades with a rotational speed of 1317 rpm. The specification of the squirrel-cage fan is presented in Table 1. In this paper, the flow at the nearly maximum mass flow rate of 0.3214 kg/s inside both models was the focus and was analyzed in detail.

Table 1 Parameters of the double-suction squirrel-cage fan

Parameters	Value
Impeller inlet diameter D_1 /mm	212
Impeller outlet diameter D_2 /mm	252
Impeller width b /mm	146
Location of the middle disk b'/b	0.36
Blade number Z	60
Impeller thickness δ /mm	0.4
Volute width B /mm	180
Volute cut-off angle θ_c /°	52
Inlet angle β_{1A} /°	90
Outlet angle β_{2A} /°	165

3. Numerical Method and Experimental Apparatus

3.1 Numerical method

In this paper, the Reynolds averaged Navier-Stokes equations (RANS) and the realizable k-ε turbulence model are employed to simulate the flow in the two models. The finite volume method and the SIMPLE algorithm are used to solve the governing equations. The grid of the impeller is generated by the ANSYS Turbo-Grid, and the other parts of the computational domains by the ANSYS ICEM. The simulations were conducted by using the ANSYS Fluent, and the post-processing was accomplished by the CFD-Post.

The governing equations for the flow are as follows:

$$\frac{D\rho}{Dt}+\rho\frac{\partial u_i}{\partial x_i}=0 \tag{1}$$

$$\rho\frac{Du_j}{Dt}=\rho f_j+\frac{\partial \sigma_{ij}}{\partial x_i} \tag{2}$$

$$\rho\frac{D}{Dt}(e+\frac{1}{2}u_j u_j)=\frac{\partial}{\partial x_i}(\sigma_{ij}u_j)+\rho u_j f_j-\frac{\partial q_j}{\partial x_j} \tag{3}$$

where ρ is the fluid density, t is the time, u is the velocity, f is the unit mass force, σ is the stress tensor, e is the internal energy and q is the heat flux. For this case, the flow velocity is very low, the air is considered incompressible and the temperature rise is neglected. Therefore, the energy conservation equation, which governs the relationship between the flow and the heat transfer, can be ignored.

Figure 4 presents the grid distribution of the fan model and Fig. 5 presents the grid distribution of the range hood model, with the diagrammatic sketch of the installed squirrel-cage fan. As shown in Fig. 6, the grid distribution of the squirrel-cage fan for both models is the same.

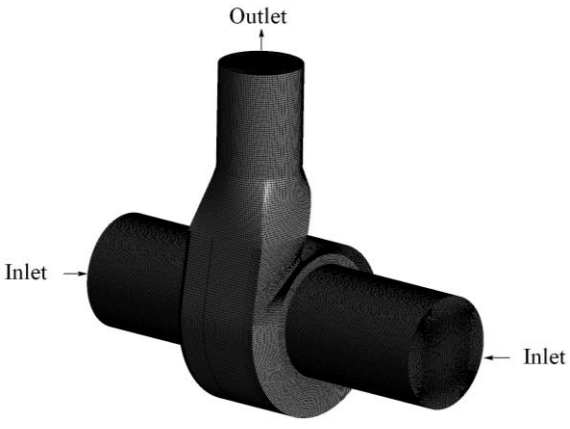

Fig. 4 Grid distribution of the fan model

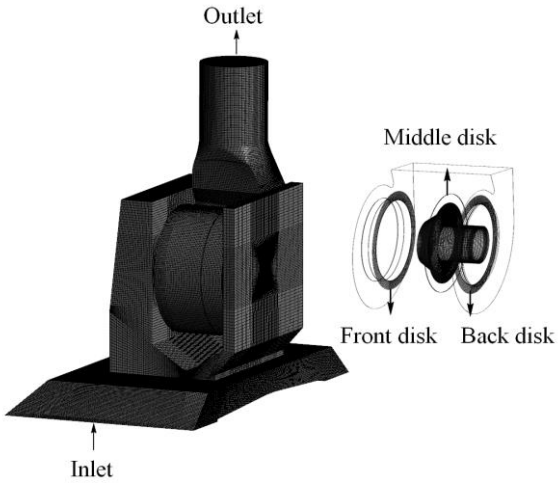

Fig. 5 Grid distribution of the range hood model

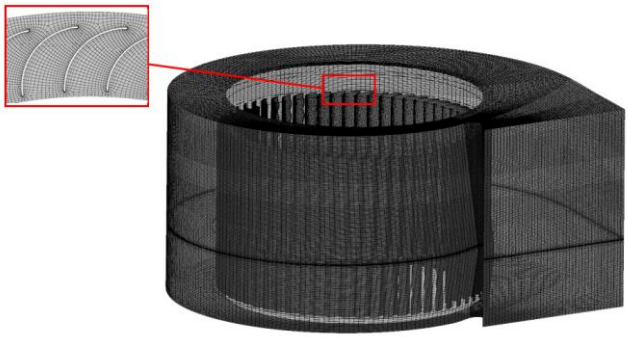

Fig. 6 Grid distribution of the squirrel-cage fan

For the fan model and the range hood model, the same inlet and outlet boundary conditions are applied, i.e the mass flow rate for the inlet boundary and the static pressure for the outlet. The air temperature is set to 25℃ to keep the air density as 1.2 kg/m^3. No-slip condition is adopted for the hydraulically smooth solid walls in the above two models. Frozen-Rotor method is used in the treatment of the interface between the rotating and stationary domains. The numerical simulation is considered to be convergent when the total pressures of the inlet and the outlet are both stable. Grid-independence validation for the range hood model was carried out at a flow rate of 0.1367 kg/s, which corresponds to the best performance point of the fan model. As shown in Fig. 7, the total pressure of the range hood model, defined as the total pressure difference between the outlet and the inlet of the range hood model, is almost unchanged when the grid number is greater than 5,500,000, which can be considered that the grid-independence solutions are obtained. In the following simulations, the grid number of the range hood model is set to 6,500,000 to ensure a reliable result. In such a grid distribution, the grid number for the volute of the fan is about 1,500,000 while the impeller is about 3,000,000. For the fan model, the grid number and distributions of the squirrel-cage fan and the ventilation duct are the same as the range hood model.

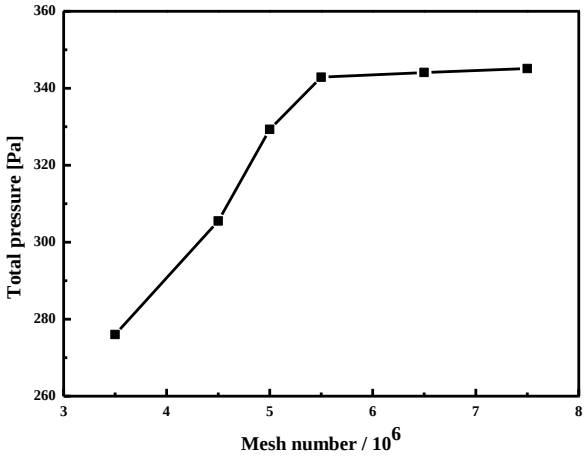

Fig. 7 Grid-independence validation for the hood model

3.2 Experimental apparatus

The aerodynamic performance of the range hood model was measured according to the GB/T17713-2011 standard [16]. The experimental apparatus of the range hood model is shown in Fig. 8. The schematic diagram of the aerodynamic performance test apparatus is presented in Fig. 9. The ventilation duct of the range hood model is connected to the experimental apparatus via a connector. The outflow of the range hood model passes through the rectifier, the diffusion section, and the regulator one by one, and finally flows out of the pressure relief cylinder via the orifice. The flow rate can be altered by adjusting the orifice at the end of the duct. The average value of the hydrostatic pressure is measured from the four evenly distributed monitoring holes. The rotational speed of the impeller was measured by a stroboscope with a resolution of 1 rpm. Finally, the volume flow rate and the total pressure of the range hood model can be calculated according to the eq. (4) and eq. (5) in the GB/T17713-2011 standard, respectively.

$$q_v = 1.111 \times ad^2 \times \sqrt{\frac{P_{s6}}{\rho_a}} \tag{4}$$

$$P = P_{s6} + K\frac{\rho_a}{2} \times \left(\frac{4q_v}{\pi \times D_4^2}\right)^2 \tag{5}$$

where q_v is the volume flow rate, a is the flow coefficient of the orifice, d is the orifice diameter, P_{s6} is the static pressure obtained by the hydrostatic pressure holes, ρ_a is the air density, P is the total pressure, K is the constant, D_4 is the rectifier diameter.

Fig. 8 Aerodynamic performance experimental apparatus

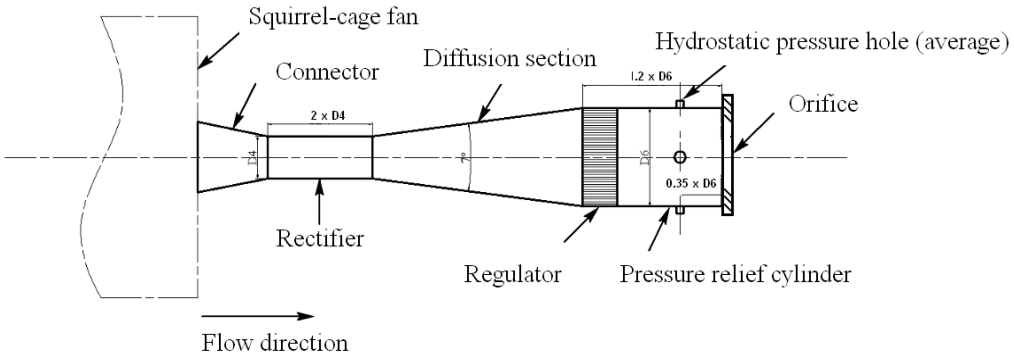

Fig. 9 Schematic diagram of the aerodynamic performance experimental apparatus

4. Results and Discussion

4.1 Aerodynamic Performance Analysis

The aerodynamic performances of the range hood model and the fan model at different flow rates were simulated by using the aforementioned numerical methods. The experimental results of the aerodynamic performance of the range hood model were also obtained on the experimental apparatus. To make a comparison, the numerical results of the fan model and the range hood model and the experimental data of the range hood model are shown in Fig. 10. In this paper, the total pressures of the two models are defined as the total pressure difference between the outlet and the inlet for both models respectively. It can be seen clearly that the total pressure of the range hood model agrees well with the experimental data, while the total pressure of the fan model is obviously higher than that of the range hood model. It demonstrates that the effects of the guiding tank on the aerodynamic performance of the range hood model can't be ignored.

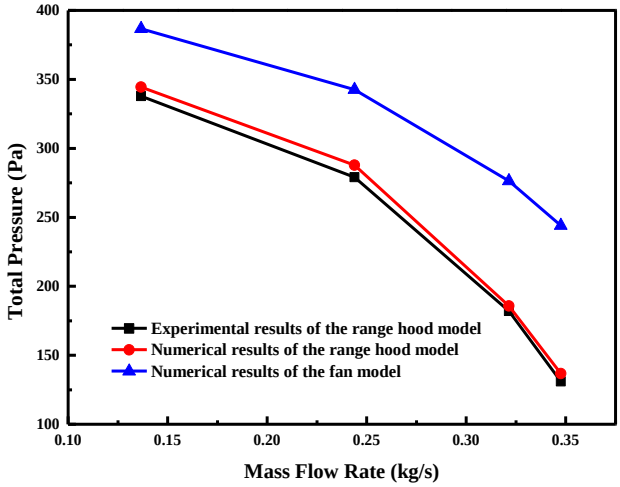

Fig. 10 Aerodynamic performance of the experimental and the numerical results

The reduction in the total pressure of the range hood model may be caused by the flow losses in the guiding tank or due to the distorted incoming flow of the fan. Because the size of the range hood model is strictly limited, it is interesting to know which of the two factors weighs heavier in the reduction of the total pressure. Therefore, the aerodynamic performances of the fan model and the fan inside the range hood model (referred to as fan-in-hood thereafter) are presented in Fig. 11. In Fig. 11, the total pressure of the fan-in-hood is defined as the total pressure difference between the outlet of the range hood model and the inlet of the squirrel-cage fan in the range hood model. For the range hood model, the flow losses in the guiding tank, defined as the total pressure reduction between the outlet and the inlet of the guiding tank, are large and cannot be ignored. However, for the fan

model, the total pressure reduction between the outlet and the inlet of the inlet tube is very small, which can be ignored. It can be supposed that the total pressure reduction between the range hood model and the fan-in-hood is caused by the flow losses in the guiding tank and the total pressure reduction between the fan-in-hood and the fan model is caused by the distorted incoming flow.

It can be seen that the total pressure of the range hood model is lower than that of the fan-in-hood when considering the flow losses in the guiding tank. Moreover, with the mass flow rate increasing, the flow losses in the guiding tank increase. Besides, the total pressure of the fan-in-hood is lower than that of the fan model, which ascribes to the distorted incoming flow caused by the guiding tank. Meanwhile, the total pressure reduction is also increasing when the mass flow rate increases. As shown in Fig. 11, at different mass flow rates, the total pressure reductions caused by the distorted incoming flow are larger than the flow losses in the guiding tank. It demonstrates that the influence of the distorted incoming flow caused by the guiding tank overweighs the influence of the flow losses in the guiding tank for the overall aerodynamic performance of the fan-in-hood. To conclude, with the consideration of the actual incoming flow, the range hood model is better to describe the actual case. The analysis of the distorted incoming flow effects on the flow characteristics and aerodynamic performance of the squirrel-cage fan is needed.

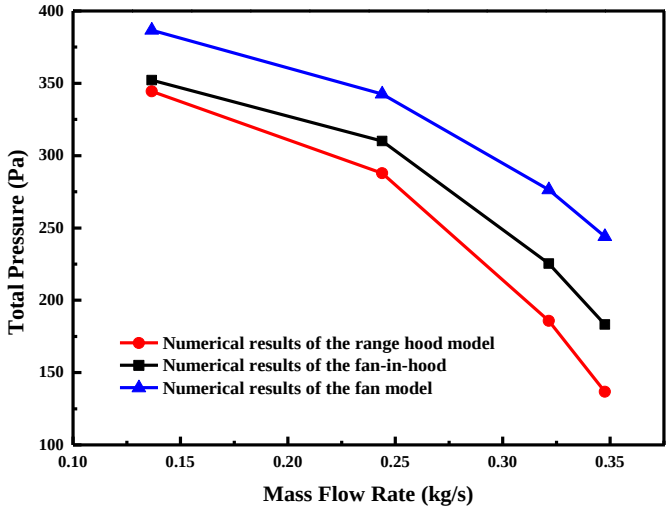

Fig. 11 Aerodynamic performance of the numerical results

4.2 Flow Characteristics Analysis

To further verify the differences of the flow characteristics between the fan model and the range hood model, analysis of the flow characters along the flow path of the air in the range hood model at the nearly maximum mass flow rate of 0.3214 kg/s is given. The velocity mentioned below is the relative velocity.

Velocity streamlines inside the guiding tank are presented in Fig. 12. It is obvious that the flow in the guiding tank is distorted. The velocities near the outlets of the guiding tank are uneven, where the velocity close to the outlet bottom is higher than that for the top side. Besides, the flow near the front disk is distorted obviously and the deflection angles at different positions are different. The velocity near the back disk is increasing significantly due to the smaller cross section of the guiding tank. The flow distortions would further influence the flow fields and the aerodynamic performance of the squirrel-cage fan.

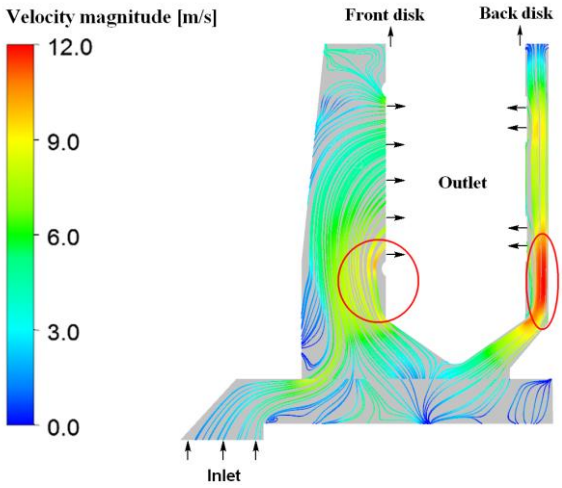

Fig. 12 Velocity streamlines inside the guiding tank

To further understand the effects of the flow distortions inside the guiding tank on the incoming flow of the squirrel-cage fan, the velocities at both inlets of the squirrel-cage fan are presented in Fig. 13. It can be seen that the incoming flow of the fan-in-hood is more distorted than that of the fan model. Affected by the flow distortions of the guiding tank, the flow fields near the fan inlets are obviously distorted. The velocities near the bottom of the fan inlets are much higher than those of the fan top side. In addition, at the fan inlets near the back disk, the lower velocity regions appear near the volute tongue.

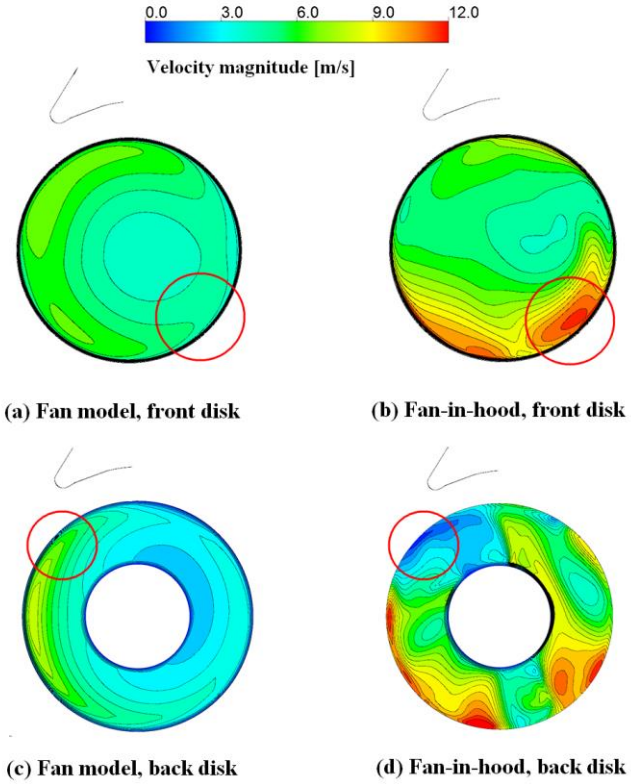

Fig. 13 Velocity contours at both inlets of the volute

Figure 14 gives the incoming flow velocity distribution, and the velocity directions of the incoming flow are analyzed. For the fan model, the air flows into the squirrel-cage fan along the axial direction, which has a more uniform distribution. However, for the fan-in-hood, the air flows into the squirrel-cage fan with a certain deflection angle, and the deflection angles are different for both front and back sides. Moreover, the secondary flow inside the volute is related to the impeller outflow velocity directions. For the fan-in-hood, the velocity directions of the impeller outflow will be distorted due to the inlet distortions caused by the guiding tank, which will worsen the local flow characters in the volute.

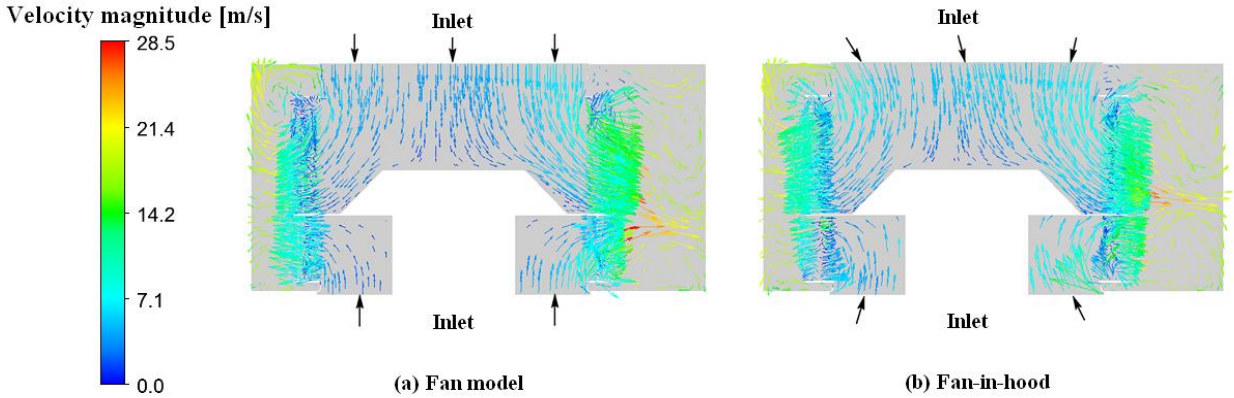

Fig. 14 Velocity vector inside the volute

As can be seen in Figs.13 and 14, significant changes in both magnitudes and directions of the velocity can be seen clearly at inlets of the fan-in-hood. It can be suggested that the incoming flow of the fan-in-hood is distorted due to the guiding tank and the inlet distortions will further influence the flow characteristics of the squirrel-cage fan.

The velocity streamlines at 50% span of the impeller near the front disk for the fan model and the fan-in-hood are presented in Fig. 15. In the fan model, as shown in Fig. 15 (a), it can be seen that the velocity streamlines in every impeller passage show a uniform distribution. In detail, obvious secondary vortices are observed near the suction surface and are distributed uniformly near the leading edge of impeller. The similar velocity streamlines distribution in the fan model may be related to its relatively uniform incoming flow, which will lead to the similar incidence angles of the flow as well as the similar incidence losses around the leading edge. However, due to the existence of the guiding tank, the incoming flow of the impeller in the fan-in-hood is distorted. As shown in Fig. 15 (b), the velocity streamlines in the impeller passages are different. Specifically, the secondary vortices appear in some passages, while is not every passage. The severe secondary vortices are observed near the volute tongue and the flows in some passages are blocked as shown in Fig. 15 (b), which would worsen the flow in the impeller and deteriorate the aerodynamic performance of the range hood model.

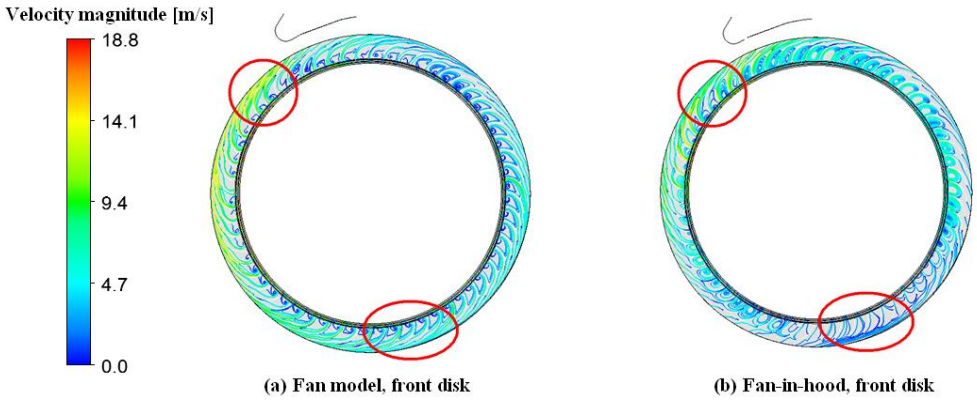

Fig. 15 Velocity streamlines at 50% span of impeller near the front disk

Figure 16 gives the static pressure at 50% span of the impeller near the back disk for both the fan model and the fan-in-hood. It can be noted that the static pressure distributions of the impeller are quite different. Obviously, the static pressure of the fan-in-hood is lower than that of the fan model. Besides, the large scale of the lower pressure regions can be seen clearly on the suction surface near the volute tongue in the fan-in-hood, which would increase the flow losses in the passages and further worsen its aerodynamic performance. The larger scale of the lower pressure regions also appears near the trailing edge of the impeller as shown in Fig. 16 (b), which would make the impeller outflow separation serious and increase the wake losses of the impeller. These differences in the static pressure illustrate the corresponding aerodynamic performance differences between the fan model and the fan-in-hood (shown in Fig. 11).

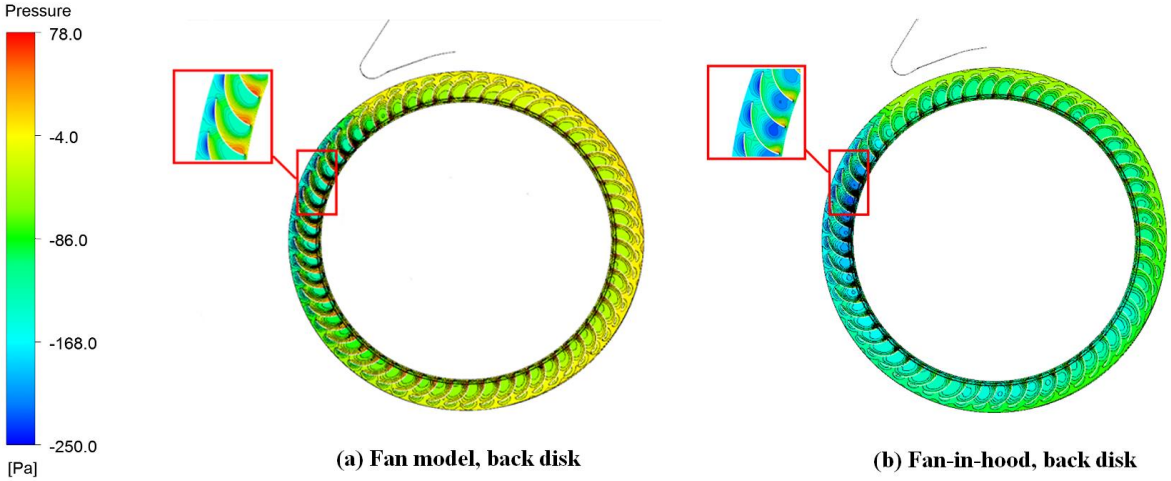

Fig. 16 Static pressure contours at 50% span of impeller near the back disk

Figure 17 presents the vortex structures with the swirling strength of 665.42 inside the volute of both the fan model and the fan-in-hood. The swirling strength is the imaginary part of complex eigenvalues of the velocity gradient tensor, which represents the strength of the local swirling motion. In Fig. 17, obvious differences are observed near the volute tongue and the back disk inlet. Vortices in the fan-in-hood are more than those of the fan model due to the inlet distortions caused by the guiding tank. However, the fan model adopts an extented straight tube as the inlet duct, which provides the uniform incoming flow. Clearly, the effects of the vortices caused by the inlet distortions on the aerodynamic performance of the squirrel-cage fan cannot be ignored.

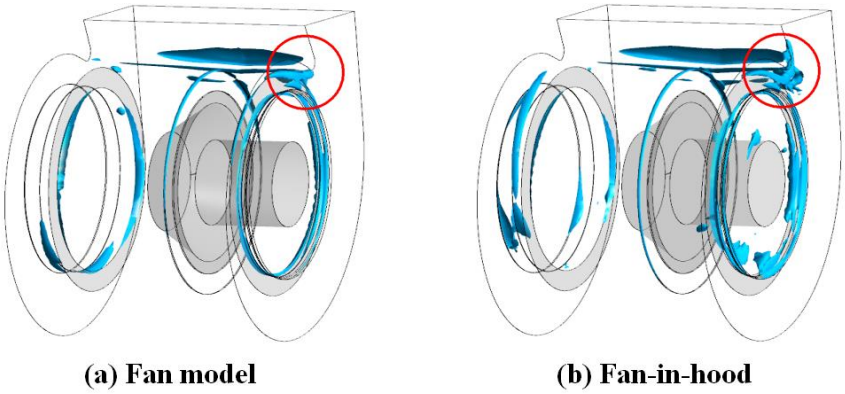

Fig. 17 Vortex core regions inside the volute

Figure 18 gives the velocity distribution at 50% span of both the fan model and the fan-in-hood. The velocity distribution near the volute can be seen a clearly difference. For the volute near the front disk, the impeller outflow velocity near the volute tongue of the fan-in-hood is lower than that of the fan model. Compared with the fan model, lower velocity regions also occur near the volute outlet of the fan-in-hood, which demonstrates that the velocity distribution of the volute outlet is also affected by

the inlet distortions. Besides, for the volute near the back disk, the impeller outflow velocity near the volute tongue of the fan-in-hood is also lower than that of the fan model, while the velocity of the volute outlet is higher than that of the fan model. Moreover, near the impeller inlet for the back disk in the fan-in-hood, a much more complex velocity distribution is observed. It can be concluded that the inlet distortions of the squirrel-cage fan make a quite difference in velocity distributions inside the volute and will affect the aerodynamic performance of the fan obviously.

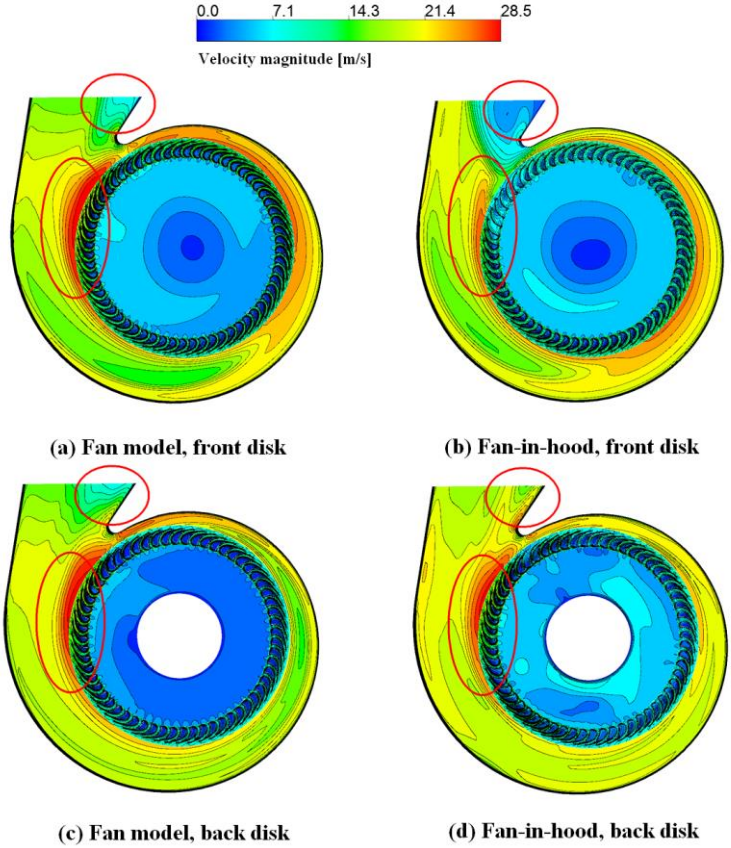

Fig. 18 Velocity contours at 50% span of the volute and impeller

The secondary flow inside the volute can be seen clearly from the velocity streamlines distribution, as shown in Fig. 19. Four obvious secondary vortices are observed inside the volute for both models. For the fan-in-hood, the vortices are more serious for regions near the middle and back disks. However, for the same positions of the fan model, the vortices are weaker and have less influence on the velocity distributions. As mentioned above, the inlet distortions will influence the impeller outflow velocity directions clearly, which creates severer secondary vortex regions.

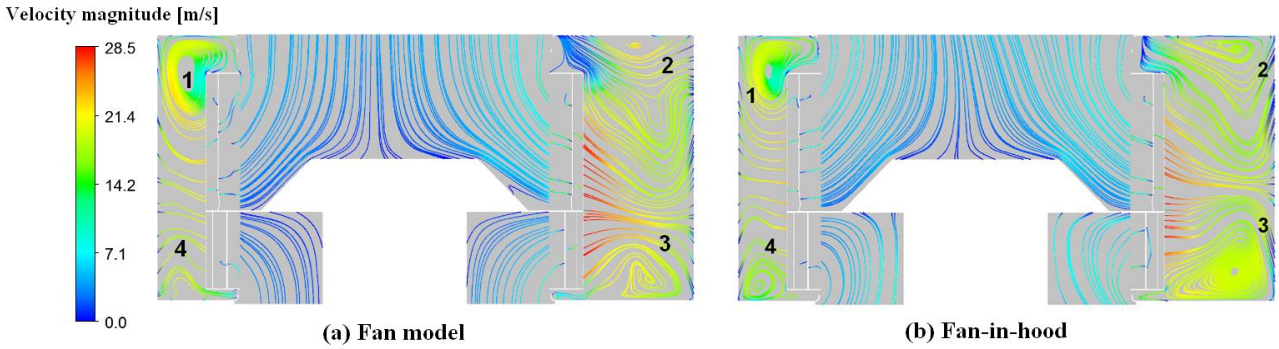

Fig. 19 Velocity streamlines inside the volute

Finally, flow fields near the collector are very sensitive to the incoming flow. Therefore, the velocity at the back of the collector is investigated in detail. As shown in Fig. 20, for the fan model, the lower velocity regions at the back of the collector have a larger scale than that for the fan-in-hood. It can be explained that in the fan model, the air flows into the volute along the axial direction, changing its velocity directions from the axial to radial near the middle and back disks. As a result, the impeller outflow near the front disk is insufficient, which leads to a larger scale of lower velocity regions near the front disk. However, in the fan-in-hood, the air flows into the squirrel-cage fan with a deflection angle, which will increase the impeller outflow near the front disk. Therefore, the lower velocity regions at the back of the collector in the fan-in-hood are smaller. To conclude, the inlet distortions would affect the velocity distributions at the back of the collector, which will further influence the aerodynamic performance of the squirrel-cage fan.

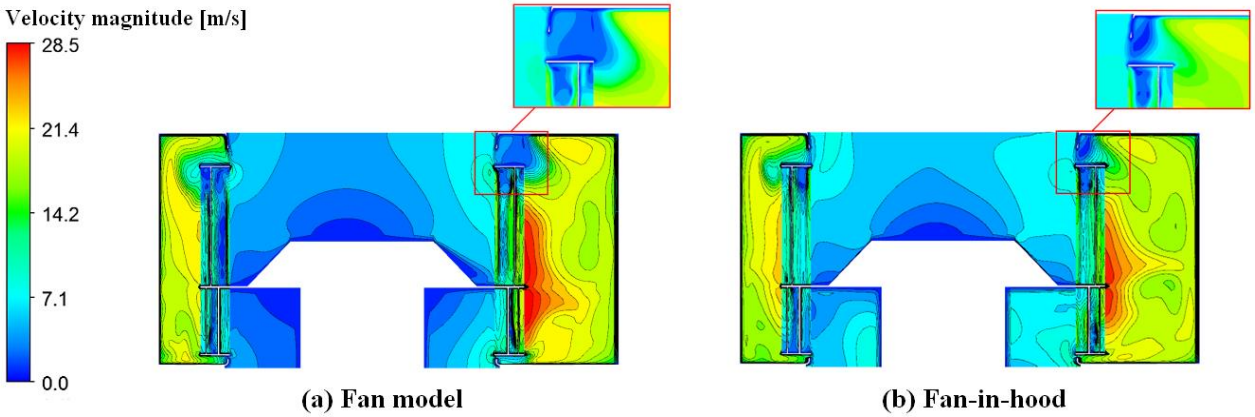

Fig. 20 Velocity contours at the back of the collector

5. Conclusion

Numerical investigation on a double-suction squirrel-cage fan of the range hood is presented in this study. Differences in the velocity, pressure and vortex distributions between the fan model and the range hood model are investigated to reveal the effects of the guiding tank on the range hood. The main conclusions can be summarized as follows:

1. The guiding tank in the range hood will cause flow losses and obvious inlet distortions, which will worsen the aerodynamic performance of the squirrel-cage fan. And the influence of the distorted incoming flow is larger than that of the flow losses in the guiding tank.
2. Due to the existence of the guiding tank, both the magnitude and the direction of the incoming flow velocity of the squirrel-cage fan in the range hood model have obvious changes compared with those of the fan model.
3. For the range hood model, the static pressure of the impeller is lower than that of the fan model. Lower pressure regions appearing near the suction surface and the trailing edge of the impeller would deteriorate the flow in the impeller and increase the flow losses significantly. Besides, severer secondary vortices appear in the impeller for the range hood model, which would cause more separation flow losses. The worse flow in the impeller not only worsens the aerodynamic performance of the impeller, but also deteriorates the flow in the volute.
4. The velocity near the volute tongue becomes lower and more vortices appear inside the volute for the range hood model, which would increase the flow losses in the volute and decrease the static pressure rise. In addition, the flow fields at the back of the collector are also influenced by the guiding tank, where the lower velocity regions become smaller due to the sufficient impeller outflow near the front disk.

Acknowledgments

This work was financially supported by the National Key R&D Program of China (2018YFB0606101) and the Natural Science Foundation of China (51876158).

Nomenclature

b	Impeller width [mm]
b'	Location of the middle disk [mm]
B	Volute width [mm]
D_1	Impeller inlet diameter [mm]
D_2	Impeller outlet diameter [mm]
m	Mass flow rate [kg/s]
P	Total pressure [Pa]
t	Time [s]
Z	Number of blades
β_{1A}	Inlet angle [degree]
β_{2A}	Outlet angle [degree]
δ	Impeller thickness [mm]
θ_c	Volute cut-off angle [degree]
ρ	Fluid Density [kg/m^3]

References

[1] Heo MW, Kim JH, Seo TW, et al., 2016, “Aerodynamic and aeroacoustic optimization for design of a forward-curved blades centrifugal fan,” Proceedings of the Institution of Mechanical Engineers Part A Journal of Power & Energy, Vol. 230, No. 2, pp. 154-176.

[2] Gholamian M., Rao GKM, et al., 2013, “Numerical investigation on effect of inlet nozzle size on efficiency and flow pattern in squirrel cage fans,” Proceedings of the Institution of Mechanical Engineers Part A Journal of Power & Energy, Vol. 227 No. 8, pp. 896-907.

[3] Gholamian M, Rao GKM, et al., 2014, “Effect of inlet diffuser diameter on flow pattern and efficiency of squirrel cage fans with CFD method,” International Journal of Fluid Mechanics Research, Vol. 41, No. 2, pp. 106-119.

[4] Darvish M, Tietjen B, Beck D, et al., 2014, “Tonal noise reduction in a radial fan with forward-curved blades,” ASME Turbo Expo, Germany, GT-2014-26253.
[5] Velarde-SuáRez S, Ballesteros-Tajadura R, Santolaria-Morros C, et al., 2001, “Unsteady flow pattern characteristics downstream of a forward-curved blades centrifugal fan,” Journal of Fluids Engineering, Vol. 123, No. 2, pp. 265-270.
[6] Samian RS, Montazerin N, Damangir A, et al., 2010, “An experimental study of squirrel cage fan rotor width on performance and velocity profiles,” International Conference on Computer & Automation Engineering, Singapore, ICCAE-2010-5451456.
[7] Kang KJ, Park JG, Shin YH, et al., 2010, “Flow characteristics with variations of cut-off angle of multi-blade fan for ventilation,” International Conference on Fluid Machinery, Kuala Lumpur, Malaysia, 732-739.
[8] Ballesterostajadura R., Francisco Israel Guerras Colón, Sandra VelardeSuárez, et al., 2009, “Numerical model for the unsteady flow features of a squirrel cage fan,” American Society of Mechanical Engineers, FEDSM-2009-78479.
[9] Zhang, R., Wang, K., et al., 2018, “Aerodynamic optimization of squirrel-cage fan with dual inlet,” International Journal of Fluid Machinery and Systems, Vol. 11, No. 3, pp. 234-243.
[10] Iwamoto, Y., Kusuzaki, R., et al., 2017, “Effect of deflected inflow on flows in a strongly curved 90 degree elbow,” International Journal of Fluid Machinery and Systems, Vol. 10, No.1, pp. 76-85.
[11] Montazerin, N., A. Damangir and H. Mirzaie, 2000, “Inlet induced flow in squirrel-cage fans,” Proceedings of the Institution of Mechanical Engineers Part A Journal of Power & Energy, Vol. 214, No. 3, pp. 243-253.
[12] Wang, N., Ding, L., et al., 2016, “Study on performance of marine centrifugal fan with inlet distortion,” Ship Engineering.
[13] Zhang, H., An, K., et al., 2018, “Influence of inlet distortion of different ranges on subsonic axial-flow compressor,” Journal of Aerospace Power.
[14] Cheah, K.W., T. Lee, et al., 2011, “Numerical study of inlet and impeller flow structures in centrifugal pump at design and off-design points,” International Journal of Fluid Machinery and Systems, Vol. 4, No. 1, pp. 25-32.
[15] Pedersen N., Larsen P.S. and Jacobsen C.B., 2003, “Flow in a Centrifugal Pump at Design and Off-Design Conditions – Part I: Particle Image Velocimetry (PIV) and Laser Doppler Velocimetry (LDV) Measurement,” ASME J. of Fluids Eng., Vol. 125, pp. 61-72.
[16] General Administration of Quality Supervision. Range Hood. Standards Press of China, 2012, Beijing.